

# Performance Prediction for Design of a Network of Skywave Over-the-Horizon Radars

David B. Francis, Manuel A. Cervera, Gordon J. Frazer, Australian Department of Defence, Edinburgh, South Australia, Australia

## INTRODUCTION

Skywave over-the-horizon radar (OTHR) is long-range beyond-horizon radar technology that is presently employed by several nations for wide-area surveillance of aircraft and maritime vessels [1]. This radar class uses propagation via the ionosphere [2] to achieve radar energy propagation to and from the target region. The ionosphere is driven by varying solar interaction with the Earth, and this variability significantly influences the operational performance of a skywave OTHR. Considerable care in selecting radar-operating parameters is required to achieve the best performance.

Australia has a network of three skywave radars known as the Jindalee Operational Radar Network [3]. These three radars have a degree of overlapping coverage and are operated jointly in a coordinated manner as a single radar network, with individual radar employed as appropriate, to achieve the overall mission objectives. Consider, for example, a mission with the goal of detecting and tracking aircraft in a particular geographical region for several days. The varying ionosphere will require judicious dynamic selection and operation of one or more of the three available radars to achieve the mission objective in the presence of the changing ionosphere.

Skywave OTHR is typically a bistatic system with separate transmitter and receiver subsystems sited 100 to 200 km apart. The separation is small compared with the radar to target range of 1,000 to 3,000 km. The radio-frequency isolation resulting from this physical separation allows radar waveform transmission to be continuous without overloading the receiver; hence, it maximises target detectability. The transmit and receiver subsystems are asymmetric with completely different transmit and receive antenna array designs. The spatial resolution of the transmit subsystem is typically one twentieth of that of the receiver subsystem (so the

transmit array is approximately one twentieth the physical size of the receiver array). The radar operates by directing a transmitter beam via the ionosphere to produce an illumination footprint on the Earth's surface at some subregion of the total potential coverage area. Multiple simultaneous receiver beams with higher spatial resolution cover the transmitter footprint. A footprint is several hundred kilometres by several hundred kilometres in area. The radar mission and the ionospheric propagation conditions govern the footprint location within the area of total potential coverage. Depending on the type of target, the radar will coherently measure within the illuminated footprint between 1 and 60 seconds. The radar will then switch the illumination footprint to some other region of total potential coverage, again based on the radar mission and propagation conditions. To establish and sustain tracks on detected targets, it is important that radar measurement of a particular target be updated, so a given illumination footprint will regularly be revisited. The radar revisit strategy depends on the target detectability and the target dynamics. For highly manoeuvring targets, the radar operator may configure the system to stare at a single footprint continuously. However, this will decrease the proportion of total potential coverage area for a given radar resource.

Operating a network of OTHR in this manner involves many considerations. These include the underlying concept of operations, ionospheric conditions, the particular level of operator experience, the number of radars and their location, the individual radar sensitivities, instrumental fidelity, and so on. When considering new surveillance applications, the question naturally arises as to how one might design a new OTHR network. The system designer has many factors that will influence their design selections. Significant design degrees of freedom are manifold. They include the operational mission and definition of success, anticipated ionospheric conditions, the number of radars and their physical locations, individual radar sensitivity and the operating parameter space of each radar, the network coordination strategy, and the total system cost.

In this article, we explore this question and propose a methodology for designing a network of skywave OTHR. We call this the *radar network design methodology*. We are also interested in OTHR networks of many individual OTHR compared with current systems with only a few radars. In this new approach, the individual radars have lower sensitivity than existing systems, and hence reduced cost, but are located as required to provide range and aspect diversity to the target region of interest. We suspect such netted-diverse-compact OTHR networks will achieve comparable

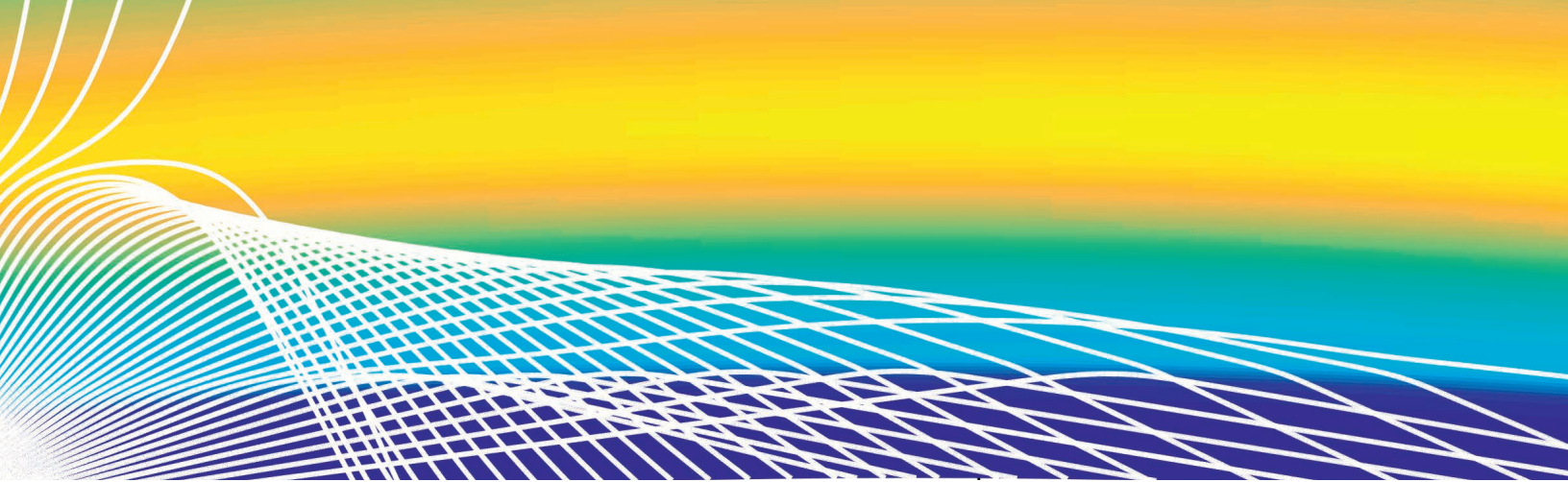
---

Authors' current address: D. B. Francis, M. A. Cervera, G. J. Frazer, Defence Science and Technology Group, Australian Department of Defence, Third Avenue, Edinburgh, South Australia 5111 Australia, E-mail: (david.francis@dsto.defence.gov.au). M. A. Cervera is also at the School of Physical Sciences, University of Adelaide, Adelaide, Australia.

Manuscript received March 2, 2017, revised September 18, 2017, and ready for publication September 22, 2017.

Review handled by D. O'Hagan.

0885/8985/17/\$26.00 © 2017 Crown



performance to present-day OTHR systems at lower total network cost, and we are using the approach described herein to explore the possibility. In this article, though, we demonstrate our methodology by using the case study of a hypothetical three-radar network located in the South Pacific and directed at eastern Australia. This example illustrates our approach for a fictional but practical case. Because the example is for illustrative purposes, we have ignored cost as a design parameter.

### OTHR NETWORK SCENARIO

We consider the specific case of a three-radar network with notional coverage, shown in Figure 1, to explore our radar network design methodology. The individual radars are located in New Zealand, Norfolk Island, and New Caledonia and are directed, with overlapping coverage, toward the eastern coastal region of Australia.

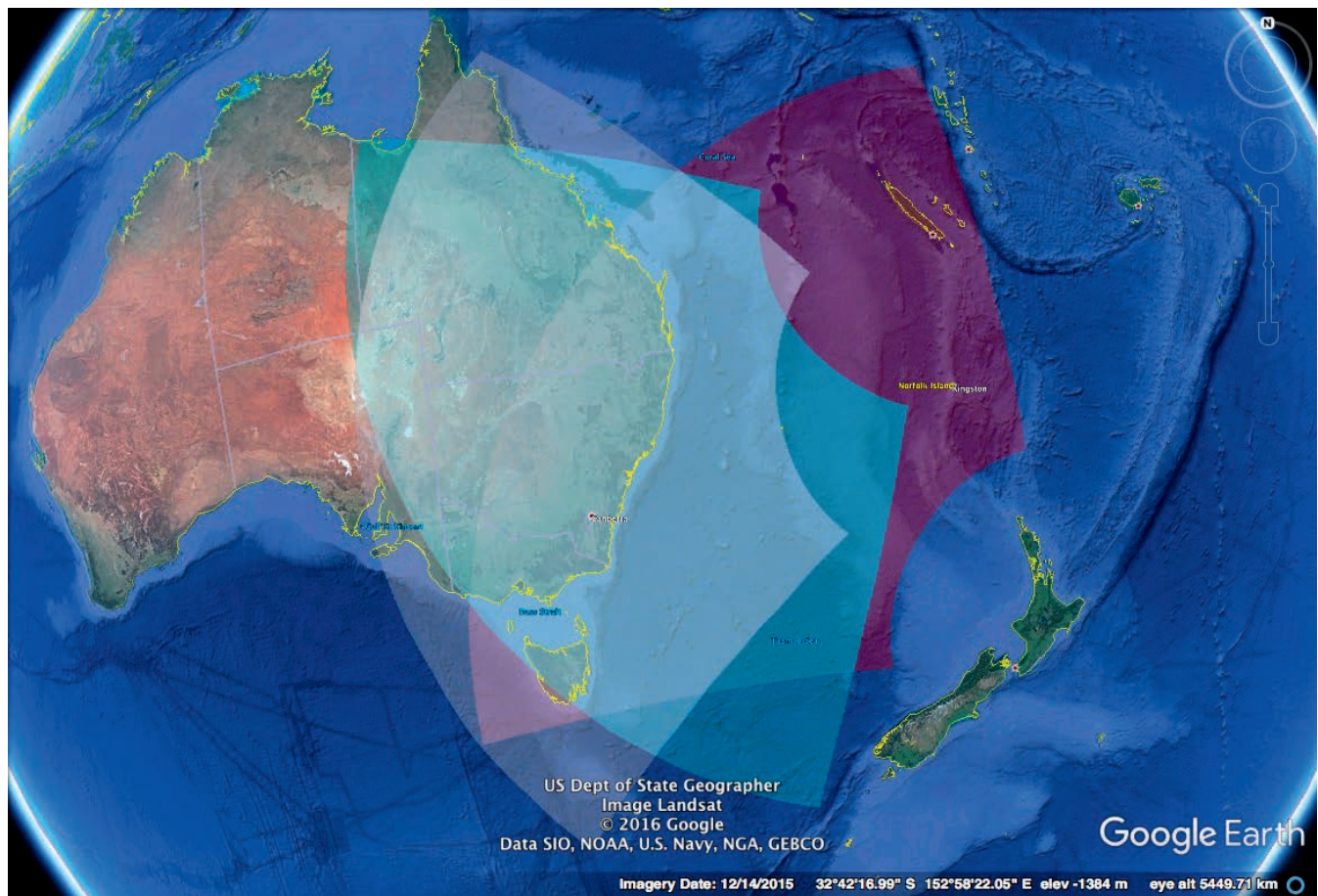


**Figure 1.**

Geographical laydowns (translucent red, white, and blue) showing regions of potential coverage for a hypothetical three radar network. The radars are located in New Zealand, Norfolk Island, and New Caledonia and directed toward Australia and have overlapping potential coverage. The regions shown are reduced at any given moment due to finite radar sensitivity and time-varying propagation support via the ionosphere.

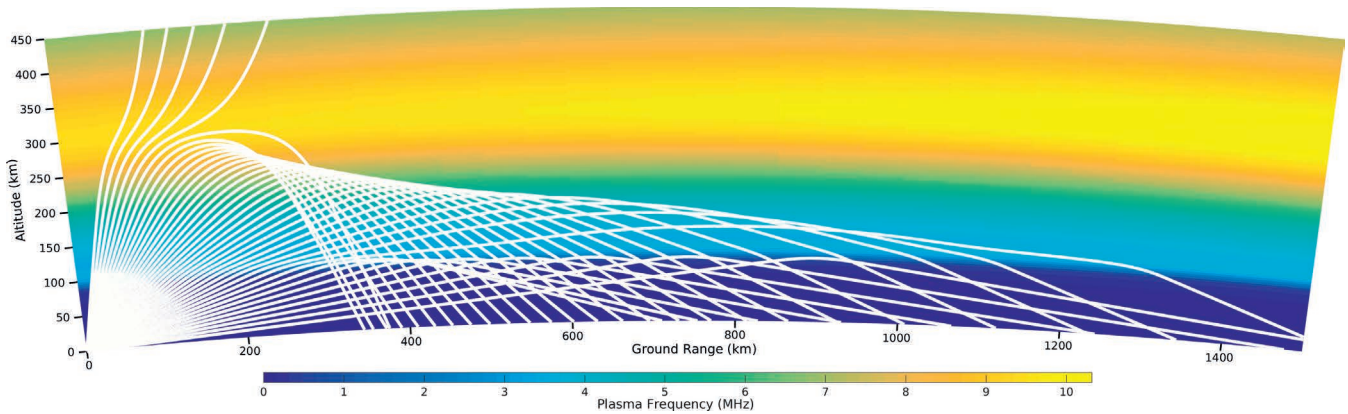


**Figure 2.**

Example of one-way ray paths for 10 MHz rays calculated by 2D numerical ray-tracing for the New Zealand radar during daytime, summer, solar maximum conditions. Note the different ionospheric propagation modes and the ionospheric penetration by the high elevation angle rays.

The notional potential coverage region for each radar has an azimuth extent of 90° and range of 1,000 to 3,000 km. OTHR generally has a large possible coverage, subject to ionospheric conditions, so this particular network arrangement will have some capability against most of the eastern half of Australia. However, the instantaneous actual coverage is moderated by time and space-varying propagation and the radar sensitivity.

## RADAR MODELLING

The performance of radar systems, such as OTHR, is governed by factors including the physical radar equipment, such as transmitter power and transmit and receive antenna gain, the selection of signal and data processing algorithms, the waveform scattering properties of the target and any unwanted scatterers (called clutter), and the physical operating environment governing radar signal propagation support and level of external noise encountered by the radar receiving system. OTHR relies on target motion and the Doppler effect to separate radar returns of moving targets from the backscatter from stationary land or the slowly moving sea surface. The typical range and azimuthal resolution cell size in OTHR is many tens of square kilometres surrounding the target. Earth return ground clutter is usually more than 50 dB larger than the return from an aircraft. In some cases, usually associated with particular ionospheric conditions, clutter may become spread in Doppler and extend into the non-zero Doppler detection space. In our study, we use a simplified clutter model, as described shortly.

For this case study, we consider a set of models for the radar, environment, target, and values for operational parameters. These are all intended to be examples to allow us to demonstrate the radar network design methodology. We intend the reader to be able to use their own models or parameters, as appropriate, to answer their own performance analysis questions using the metrics developed in the follow sections.

With OTHR, the available radar transmit power and transmit and receive antenna gain are fixed for a given installation; the signal and data processing algorithms are specified and generally fixed (although may adapt dynamically to the propagation, clutter, and noise environment); and target scattering properties are either

pre-measured, modelled, or unknown for any target that may be detected. The radar signal propagation and external noise environment is highly varying, and any model-based predictor of OTHR performance must incorporate this variability, although as noted, we do assume the receiver system to be externally noise limited. We model each of these aspects independently in our approach.

A model of the environment in which an OTHR operates requires contributing models of the propagation of the transmitted signal to the target and clutter sources and return to the radar receiving system. It also requires knowledge of the external noise environment at the radar receiving location and a measure of the Earth backscatter from the region surrounding the target.

In our case study, we choose the transmit antenna to be a linear array of eight log-periodic dipole curtain elements, with an interelement spacing of 6 m. We specify the individual per-element power-amplifiers to be capable of up to 5 kW of peak power per element. The receiving array is designed to be a linear array of 64 doublet elements, with an interelement spacing of 6.4 m and the doublet design detailed in [4]. Doublets, in this case, are defined to be two monopole antennas with one phase-shifted by  $\pi$  radians and then combined to gain directivity perpendicular to the length of the linear array and provide a null in the reverse (non-transmit) direction. Both arrays are designed to operate in the bandwidth of 13 to 26 MHz. This frequency limitation reduces the design cost of the radar as transmit operation at lower frequencies typically requires an additional separate transmit array of size, and hence cost, scaled to the lower frequency range of operation. All arrays are directed to have array boresight maxima directed toward Sydney (SYD), Australia. They are modelled by using a method-of-moments electromagnetic (EM) solver (Numerical Electromagnetics Code-4 [5]). We note that we do not require a model for the internal noise of the receivers because, for well-designed high-frequency (HF) radar receiver systems, the system internal noise will be lower than the external noise impacting the receiver.

Ionospheric propagation is modelled by using radio wave ray-tracing methods applied to the International Reference Ionosphere (IRI) [6]. In our work, we use the ray-tracing toolbox (PHaRLAP) [7], developed by one of the authors. Figure 2 displays an example of one-way ray paths calculated by using PHaRLAP's two-dimen-

sional (2D) numerical ray-tracing engine. It is beyond the scope of this article to discuss the physics describing the effect of the morphology of the ionosphere on the ray paths; however, we note that there is often more than one propagation mode to a particular ground range. In general, for a quasi-monostatic system, if there are  $N$  propagation modes to a target, then there are a total of  $N^2$  modes that are available to return energy to the receiver. Each of these modes will have an associated group (or radar) range, elevation angle at the receive array, and power loss.

To characterise the signal propagation properties of each radar in the proposed network, we calculate propagation look-up tables over a range of environmental conditions: this includes the equinoxes and solstices at low, medium, and high solar activity levels. The Zurich smoothed sunspot number (SSN) is a measure of the solar activity [2] and used in the IRI model. For this case study, we present results using low and medium solar activity of SSNs 20 and 70, respectively. Ionospheric propagation effects, such as ray focusing [2] and HF radio wave absorption, are included. The ionospheric absorption model is from George and Bradley [8], which varies across solar activity, season, time of day, spatial location, and the angle of the ray path taken.

The look-up tables take the form of predicted received power from a 1-W radiator, assuming a 1-second coherent integration time (CIT) and a target with 1-m<sup>2</sup> radar cross section (RCS). The tables are parameterised by ground range and radar operating frequency, with array gain included. As noted previously, there may be several propagation modes to a particular ground range; only the strongest mode for each ground range is retained for the construction of the tables. Figure 3 displays graphically propagation tables for the New Zealand radar over a range of ionospheric conditions.

This figure demonstrates the significant impact ionospheric conditions have on the frequency variability of OTHR propagation. The ionosphere is weakest at pre-dawn during winter at solar minimum, where in the top right of Figure 3, there is no propagation support at all for frequencies above 10 MHz. Propagation modelling (not shown here) indicates that an OTHR at this location would have to operate at frequencies near 5 MHz during these conditions. This would require a dual-band transmit array design that would increase the complexity and cost of the system, as mentioned earlier.

Anticipated target signal-to-noise ratio (SNR) is calculated from the propagation tables by scaling the power by the radar transmit power and CIT, using a frequency- and aspect-sensitive target RCS model, and a location-, time-, and frequency-dependent background noise model. We choose the frequency that maximises the return power over the radar processing area. This frequency is typically close to the “leading edge,” where skip focusing occurs [2]. The frequency choice is additionally restricted to be slightly less than the leading-edge frequency. This is to emulate how OTHR are operated in practice, where operating frequencies too close to the leading edge leave the radar susceptible to losing propagation support if the ionospheric conditions change rapidly, such as at times around the dusk terminator or due to ionospheric disturbances.

In this article, the RCS is characterised by using analytic estimates of a commercial airliner over different aspect angles [9]

justified using EM modelling [5]. For the noise estimate, we used a rural ITU median model for the background noise at the radar sites [10], although more sophisticated models can be used if desired [11].

We assume a simple ground clutter model with uniform backscatter coefficient  $\sigma_0$  (Earth RCS per unit area of Earth illuminated), where the clutter is confined to a Doppler band corresponding to no more than  $\pm 25$  knots. This is a valid model for an undisturbed ionosphere and the assumption that operators correctly select the radar operating frequency. If the target radial speed is less than 25 kn, then we assume it has been obscured by the ground clutter and will not be detected. In any given OTHR location, there are likely to be periods of Doppler-spread clutter that will reduce our estimates of system performance; however, we consider that to be a second-order issue for most cases within our task of overall OTHR network design. Investigating the consequences of, and provision for mitigation methods required for, Doppler-spread clutter is location dependent. For example, the impact of Doppler-spread clutter can be ignored at first-order for an OTHR network located at mid-latitude, although it will dominate performance estimates if located close to the southern or northern Aurora.

The most important parameter for OTHR tasking is the operating carrier frequency of the radio waves transmitted [3]. In a surveillance mission, we can split the area of regard into a set of radar “tiles” [12]. The tiles are the range and azimuth extent processed by the radar in each observation, as modern HF radars are fully digital coherent phased array radars. For each tile, we determine the optimal carrier frequency that maximises the energy received by propagation from the tile. This is an optimisation over SNR. One may extend the frequency optimisation to include directional noise and an external large signal environment using the models in [11], [13].

Typical OTHR waveform parameters are specified to determine additional gain and loss through the radar signal processing. We assume the use of a linear frequency modulated continuous waveform with a CIT of 4 seconds, noting that up to roughly 2 minutes is propagation coherent [1]. An additional signal processing loss of 10 dB is included as representative of losses incurred by tapering [1] used on directional transmission tapers, clutter windowing in Doppler, target windowing in range, and spatial rejection windowing in azimuth.

In summary, we assumed the base-system for each radar in the network has transmitter power of 40 kW, an eight log-periodic dipole transmit array, and 64-element doublet receiver array. Subsequently, we shall consider radar configurations with increased sensitivity. In these cases, we assume that higher radar sensitivity is achieved by employing one or more of increased transmitter power, a higher gain transmitter array containing more elements, or a higher gain receiver array containing additional antenna elements. Note that these changes may have follow on performance effects requiring performing array modelling again, and the cost of each of these options may not be equal.

We combine all the parameters so far into an estimate of SNR of the target in the detection stage of the radar system, as described in Equation (1). This equation is presented in log-scale, as the traditional parametric radar equation does not simply scale when ad-

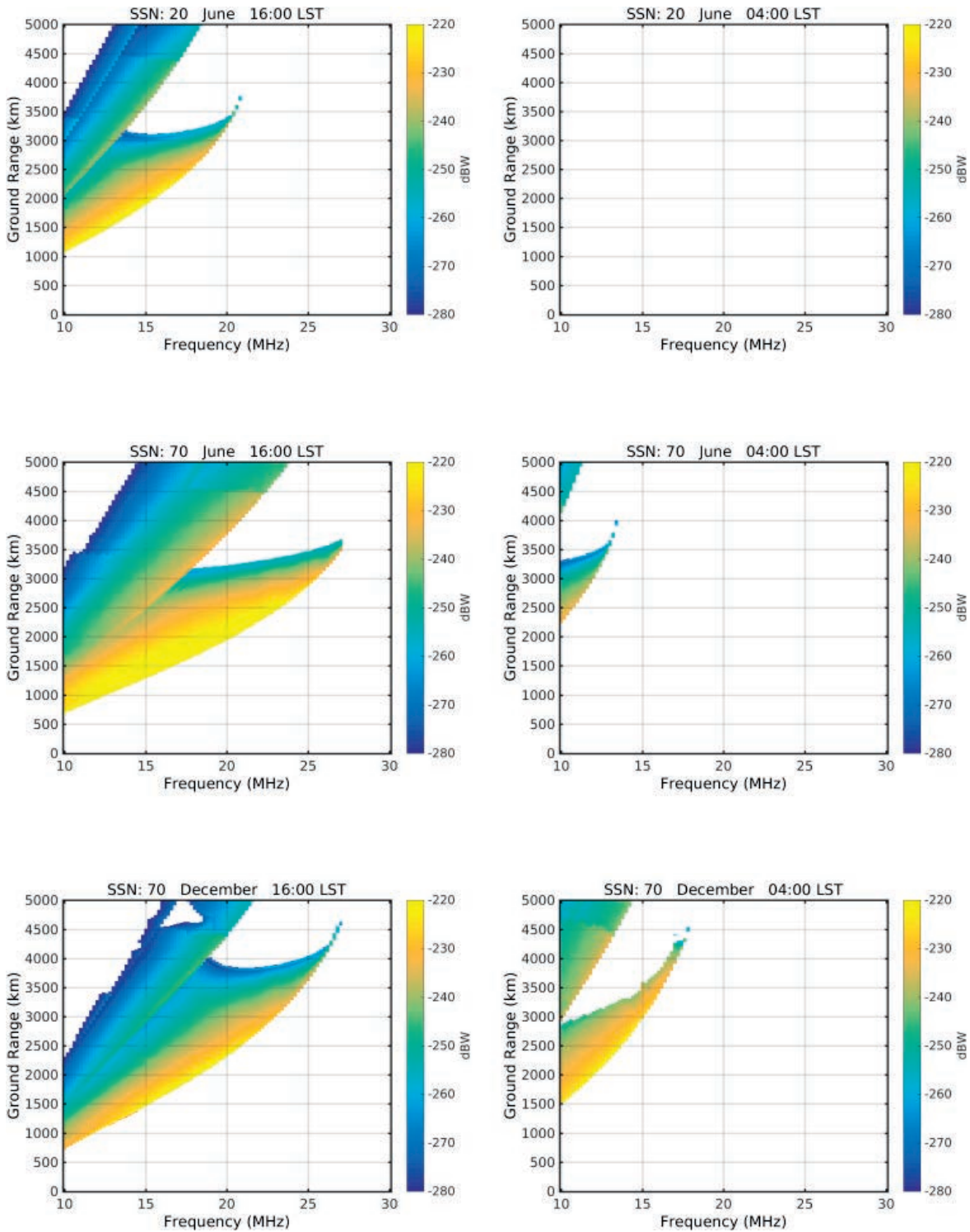


**Figure 3.** Example of daytime (left column) and nighttime (right column) HF propagation conditions during winter, low solar activity (top row); winter, medium solar activity (middle row); and summer, medium solar activity (bottom row). Note the lack of propagation support during winter at low solar activity levels. The time standard for these plots is local solar time, the local time adjusted to true solar midday.

ditive noise scaled to transmitter power are considered. This occurs when detecting targets against spread-clutter or unwanted targets, such as meteors, and will not be discussed in this particular case study but is potentially an important consideration for other use case studies. We compute

$$\text{SNR (dB)} = T_{\text{cit}} + P_{\text{tx}} + \sigma_{\text{res}} + G_p + G_m - L - n, \quad (1)$$

where  $T_{\text{cit}}$  is the coherent integration gain in dB relative to 1 second,  $P_{\text{tx}}$  is the transmitter power gain in dBW,  $\sigma_{\text{res}}$  is the target RCS in dB relative to 1 m<sup>2</sup>,  $G_p$  is the base-system propagation path and array gains generated by ray-tracing, as described previously in units of dBW per m<sup>2</sup> per s per W,  $G_m$  is an introduced marginal system gain (i.e., above the base-system) in dB as described later,  $L$  is the signal processing losses in dB, and  $n$  is the combination of external noise power and receiver noise power in dBW. Spread Doppler clutter power can also be incorporated although in the scenario discussed in the article; this is an insignificant contribution.

For all targets that are not obscured by clutter, we model the data processing step of peak detection. Detection is a statistical test producing the probability of the target signal power being greater than the threshold within a noise distribution [14]. We use an empirically derived summation of Gaussian and a log-normal distributed noise distribution to encapsulate the short time normal noise fluctuations and the less probable higher power noise events, such as lightning. The probability of false alarm is the probability of the noise power being greater than the threshold.

Once the probability of detection and false alarm are calculated for each point in space-time, we determine the probability of tracking a target. As we have targets moving through spatially fluctuating SNR values, we also have fluctuations of the probability of detection. This variation requires an exhaustive search of possible detections and misses to characterise the ability to initiate a track, i.e., it is not a simple look-up table of SNR for detection probability to track probability. We choose a characteristic  $M$  detections out of  $N$  observations model for tracking [15], where for this case study, we use  $M = 7$  and  $N = 10$ . This model declares the presence of a track if at least  $M$  out of the last  $N$  observations detected a target. This model makes no statement of track accuracy, which is beyond the scope of this work.

As the probability of detection fluctuates spatially, the target dynamics and radar revisit rate influence the resultant probability of tracking. The optimal frequency and subsequent probability of track can only be achieved by following a path of ground range and azimuth with the respective carrier frequency that obtains minimum path loss. Because these radars are observing many targets across a spatially diverse set of locations, many carrier frequencies are required. This creates a revisit time for observation of a target based on the spatial location. This case study uses a 30-second revisit time and target velocity of 600 km/h to determine our observation locations and the resulting non-uniform sequences of probabilities of detection.

## MISSION PERFORMANCE ASSESSMENT

In our approach, there are a number of radar performance assessment metrics computed for each radar location. We use a model of

track level fusion that maximises the probability of tracking over the parameter space for each radar. We then recalculate the performance metrics for the radar network. For brevity, only the network results are presented. For this study, we assume the network operates the radars independently but performs data fusion at a track level.

For each radar, we perform the calculations described in the previous section and apply a 90% probability of target tracking performance threshold. To help communicate the performance of the radar network, we condense tracking performance into sets of characteristic metric values of the typical hours of coverage and value of each radar contribution in the network. In this case study, we have chosen our characteristic missions to be the tracking of commercial aircraft flying into and out of SYD airport from Adelaide (ADL), Brisbane (BNE), Melbourne (MEL), and Hobart (HBA). Additionally, we wish to assess the tracking performance for aircraft circling SYD airport in a typical holding pattern.

The analysis for our base-system radar design shows that there is almost no coverage at low solar activity and only flight specific coverage for medium solar activity. This sensitivity is assessed as not satisfactory for the mission requirement of tracking flights to SYD.

To investigate what scale of radar sensitivity within the network would achieve the desired mission, we introduce  $G_m$ , the marginal system gain, as a sensitivity-free variable in Equation (1). We calculate the metrics described in the following section over a set of radar system sensitivity levels or marginal system gain values. These sensitivity modifications can be incorporated across the radar design and used to investigate performance stability. For example, doubling of the receive array size or doubling of the transmitter power each achieve incremental 3-dB improvement. We test an increased sensitivity above the base-system radar sensitivity of  $G_m$  between 0 and 30 dB.

## SPATIAL HOUR COVERAGE

We demonstrate the inadequate performance of the base-system design in Figure 4, where colour represents hours of performance, with red being no coverage and green being 10+ hours a day. This image is just one combination of solar state and season but demonstrates the characteristic patchy performance. By comparison when using an additional marginal system gain of 6 dB, the flights are consistently covered, as shown in Figure 5.

The BNE flight has almost no track coverage. The difficulty with tracking the BNE to SYD flight is due to the aspect geometry of all three radars. The aircrafts in this flight path are either tangential to each radar in the radar network (i.e., lost in the ground clutter) or have poor target scatter due to the aspect dependency of target RCS.

## MOSTLY-AT-LEAST HOUR COVERAGE

We use the spatial median of hours of coverage for the target missions evaluated for each season and solar state. This is a significant, but robust, data reduction compromise that demonstrates the performance changes between different levels of solar influence. This metric value indicates that most of the target flight path will be covered by the minimum probability of achieving tracking for at

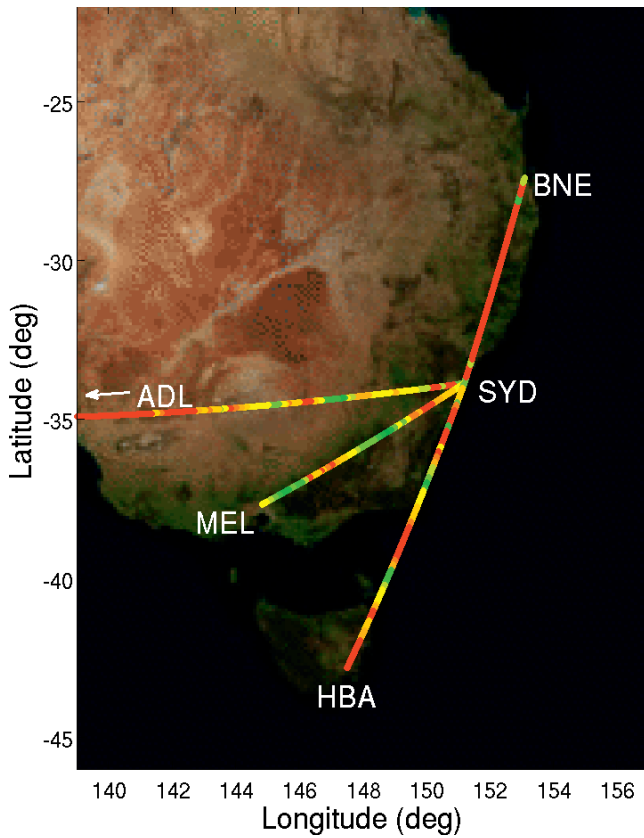


**Figure 4.** Map of eastern Australia. Shows flight routes colour coded with the predicted hours of radar network coverage for inbound to SYD flights in December with low solar activity for a radar network designed to the base-system design. Red translates to no track coverage, while green is 10+ hours of coverage a day, and yellow patches are around 5 hours of coverage.

least the resultant number of hours. This clearly identifies the seasons and solar activity levels that do not satisfy a particular system requirement of target coverage, or more generally speaking, are outside the system performance expectations. This performance metric for the scenario is displayed in Table 1 (red indicates all the conditions that produce mostly-at-least three or fewer hours of coverage). Clearly, BNE to SYD is a challenging flight to track, and the winter and spring seasons (low solar activity in the Earth-based seasonal sense) with low solar activity are difficult for all flight missions. This table allows us to investigate these poor performing parameter sets and understand what is causing the behaviour: in this case, target-radar geometry and low levels of ionisation in the ionosphere.

Although informative, the concise form of Table 1 provides no insight into the specific time of day that coverage is attained. We use an additional representation, shown in Figure 6, for the percentage of spatial track coverage as a function of hour of the day. This allows the radar network designer to identify the key hours of operation for the network.

For example, from this figure, we see that each of the candidate flights in our mission have similar hours of operation in the range of approximately 0 to 15 Universal Time (UT). We note that from 19 UT (sunrise at the ionospheric control point), there is a short increase in performance followed by a quick decline. Inspection of

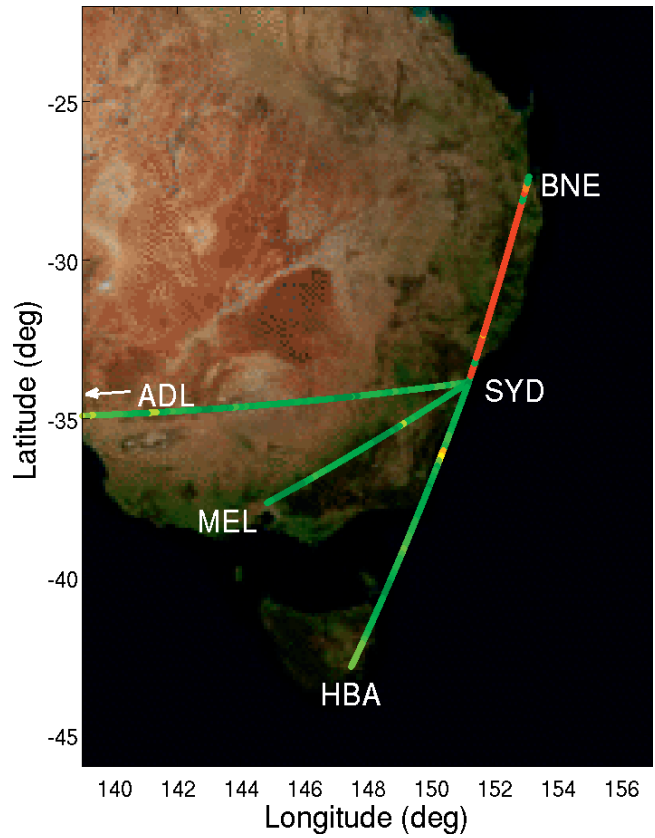


**Figure 5.** Map of eastern Australia. Shows flight routes colour coded with the predicted hours of radar network coverage for inbound to SYD flights in December with low solar activity for a radar network designed to +6 dB of the base-system design. Red translates to no track coverage, while green is 10+ hours of coverage a day, and yellow patches are around 5 hours of coverage.

the propagation look-up tables shows that this behaviour is caused by the optimal propagation frequency increasing outside of the design range of operating frequency of each radar in the network, which causes suboptimal frequency selection. We do not see this behaviour later in the day, as the well-developed ionosphere supports a much greater range of frequencies.

### RADAR SYSTEM SENSITIVITY BENEFIT AND STABILITY ANALYSIS

The radar network design methodology discussed makes many assumptions and simplifications (for example, the use of climatological models of the ionosphere [6]). We note that there are a class of variations to performance that are difficult to use in a predictive model, such as shortwave fade-outs caused by solar flares. However, there are the day-to-day variations in the noise levels and the solar activity level driving the ionosphere. We consider it important to include an assessment of the robustness of our radar network design to these non-impulsive fluctuations in sensitivity. For instance, will a small change in radar sensitivity mean overall network performance is compromised, or is there some margin for error?

Table 1.

Radar Network Spatial Median Hours (out of 24) Coverage Results for Radar Network Designed to +6 dB for Base-System Design						
SSN	Month	ADL-SYD	BNE-SYD	MEL-SYD	HBA-SYD	SYD holding
20	March	6	0	9	6	12
	June	3	0	5	3	9
	September	0	0	0	0	3
	December	11	0	12	10	16
70	March	19	1	19	18	21
	June	11	1	12	11	13
	September	17	0	18	16	20
	December	20	0	20	20	23

NOTE: Red cells illustrate undesirable performance.

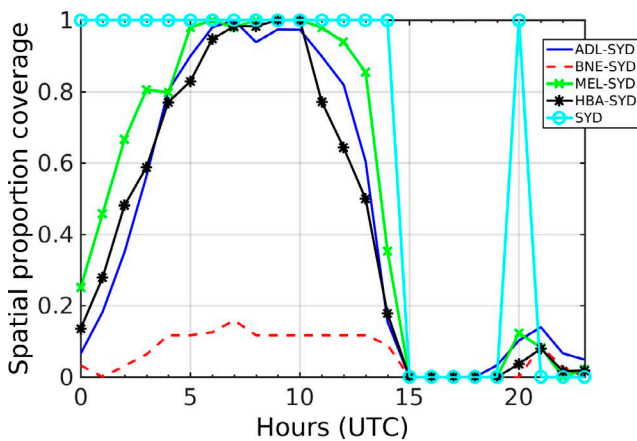


Figure 6.

Proportion of track coverage versus time of day (UT) for a radar network designed to +6 dB with respect to the base-system design for the case of operation in December and at low SSN.

What we seek in our analysis is to select a radar design sensitivity that meets the desired median performance outcome but is not a minimum design to avoid a performance “cliff” or has the radar over-designed above a performance “plateau.” The former case could result in a complete loss of capability from day-to-day variability for the climatological environmental models used. The latter case results in an overspecified radar network, leading to a higher than necessary design cost.

Using the marginal system gain as realised in the parameter  $G_m$  within Equation (1), the hours of coverage values are generated at different sensitivity levels. These performance values are compared as independent distributions of values for each season and solar activity level, where the medians are the “mostly-at-least hours coverage” metric. Statistically, we perform a two-sample  $t$ -test with unequal variance [16] to determine whether two sensitivity levels produce statistically equivalent mean hours of coverage. This is a best practice for comparing performance, as this test in-

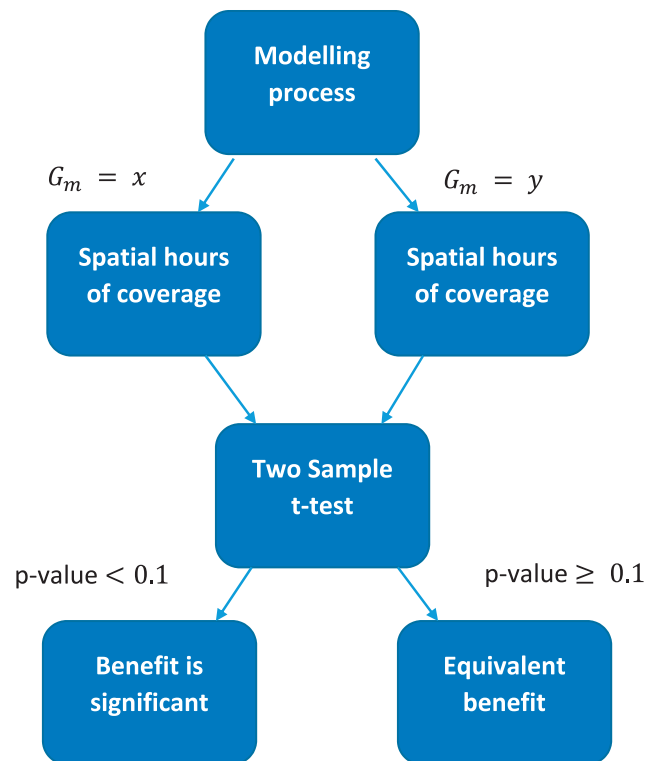
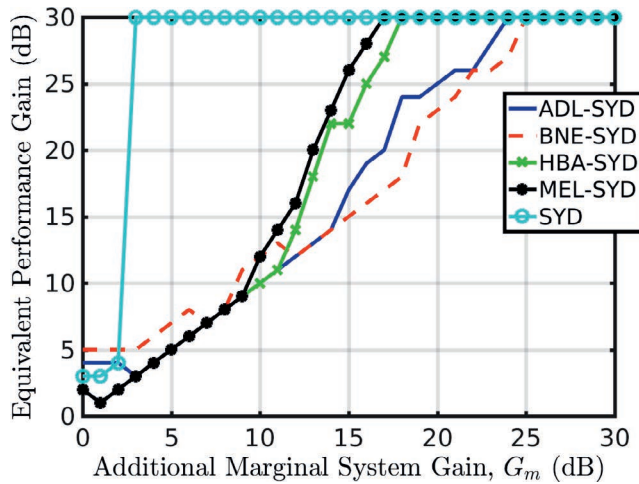


Figure 7.

The statistical testing process is performed for each combination of characteristic mission, season, and solar activity level.

incorporates the variance of performance produced by different radar designs.

For each season and solar activity level, we compare the hours of coverage distributions between each of the 0 to 30 dB additional marginal system gains. We determine that two sensitivity levels or values of additional marginal system gain are equivalent when the statistical test fails to falsify the null hypothesis of equivalent distributions. The process taken is depicted in Figure 7 as a flow



**Figure 8.** The temporal performance system gain equivalence for the radar network from 0 to 30 dB values of system gain.

diagram. For simplicity, we constrain the radar systems to have equivalent design and additional marginal system gain value. Obviously, a more global optimisation process may be conducted at great computational cost.

We incorporate the environmental conditions by taking the average of the probabilities of equivalent performance across season and solar activity level. Using these probabilities, we peruse the answer to the question: what is the minimum extra sensitivity required of the radar design to achieve a significant performance improvement? The answer is the “equivalent performance gain” for each input sensitivity or additional marginal system gain. We have displayed the equivalent performance gain value against the additional marginal system gain for the temporal and spatial performances. Figure 8 demonstrates the equivalent performance gains for each flight temporally, while Figure 9 shows the spatial equivalent performance gains.

These equivalent performance gain value curves lose the indication of absolute performance. To assess the key points of the sensitivity to performance trade-off, we must look at the mostly-at-least hours of coverage performance tables, such as Table 1.

We identify in Figure 8 that the 0 and 3 dB additional marginal system gain values are mostly equivalent, except for the SYD circling flight. Because 0 dB is the base-level radar design, we find that this is what we characterise as a performance cliff. Any radar designs with sensitivity levels near these values will produce unacceptable performance.

All the flights have their performance improved with additional marginal system gains of 3 dB and above, except for the SYD circling flight. We characterise the SYD circling flight as a performance plateau for values of 3 dB and higher, as there is no improvement in performance for the increased sensitivity levels. Note that the spatial equivalent performance curves in Figure 9 all reach a performance plateau quicker than the temporal curves in Figure 8 because the spatial locations of performance clearly split into areas of good and poor performance due to the geometry of the radars, the target geometry, and the utilisation of propagation via adequate frequency agility. Sensitivity quickly loses impact as

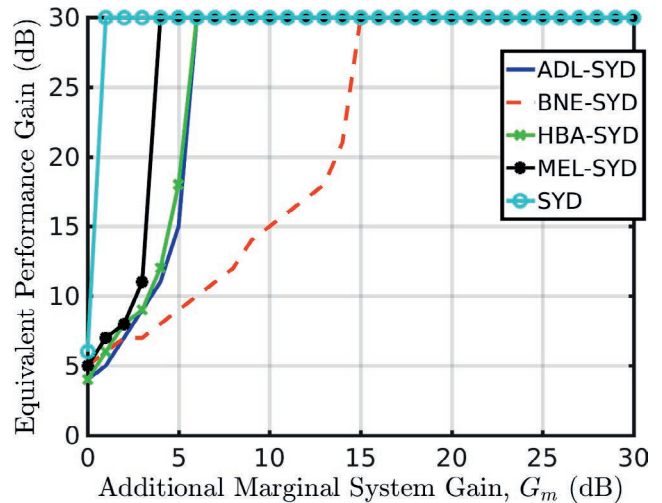


**Figure 9.** The spatial performance system gain equivalence for the radar network from 0 to 30 dB values of system gain.

these issues take dominant effect. Although, by contrast, the hours of performance have a smooth transition from no performance to good performance, as scaled by radar sensitivity, conditioned on the geometry issues not dominating performance outcomes.

Another consideration in the choice of radar design is the stability of performance. If the radar network is to overcome environmental variability, we must increase the system design above the minimum requirement, as the day-to-day propagation power may decrease or the noise may increase with respect to the monthly median environment. ITU suggests the temporal noise variation has values in the range of 5.3 to 10.6 dB [10] for residential locales. Using a temporal standard deviation of noise of 4 and 8 dB, we observe that for 6 to 11 days a month, we expect performance to be worse than a -3 dB fluctuation. This means that if we design our radar systems to a sensitivity level of an additional marginal system gain of 6 dB, we expect to fail the tracking missions 6 to 11 days a month, just based on environmental fluctuations, as the performance cliff is located at an additional marginal gain of 3 dB, resulting in the evaluated margin of a 3 dB sensitivity buffer.

We identify 6 dB as being the minimum additional system gain to achieve reasonable network performance for all but the BNE to SYD flight. This could be reasonably realised through the doubling of two of either the transmit array, receive array, or transmitter power of the reference design. This achieves most of the day performance for low solar activity and most of the day coverage for medium solar activity, as shown in Table 1. This system gain also maximises the spatial performance of the radar network, if we abandon the BNE to SYD flight mission. We expect the environmental variation to significantly reduce performance for 6 to 11 days a month.

**NETWORK PERFORMANCE ASSESSMENT**

We have identified that our radar network design is not suitable for achieving all the flight missions. Now, we may investigate the *marginal utility* each radar provides to the success of the missions

Table 2.

Percentage Radar Utility for a Radar Network Designed to +6 dB for Base-System Design for Low SSN						
Radar	Month	ADL-SYD	BNE-SYD	MEL-SYD	HBA-SYD	SYD holding
New Caledonia	March	38	5	49	64	52
	June	20	0	43	60	62
	September	27	0	63	80	100
	December	35	3	46	63	52
New Zealand	March	31	90	21	19	22
	June	46	100	19	22	22
	September	52	0	0	20	0
	December	35	96	25	18	28
Norfolk	March	31	5	31	18	26
	June	34	0	38	18	16
	September	20	0	37	0	0
	December	30	1	29	19	20

**NOTE:** Red cells illustrate the conditions in which a radar is contributing above equal value in the network.

and determine if, perhaps, we may remove one radar and locate it elsewhere to supplement weak missions, such as the BNE to SYD flight, or reduce the mission scope and remove a radar to reduce the overall network design cost.

This provides a straightforward means of assessing the relative importance of each radar in the network for each mission and can provide guidance to, for example, the order in which the radars within the network are constructed or the eventual management of operations of the radars in a coordinated network sense.

## RADAR UTILITY

Radar utility is calculated as the percentage of space-time that a particular radar is superior in the network conditioned on achieving the mission for the given operating environment. For each solar activity, season, and characteristic mission, this metric indicates which radar system is most important, or alternatively, what a proposed radar in the network offers in comparison to other radars in the network.

We demonstrate the radar utility for an additional marginal system gain value of 6 dB in Table 2. In red are the conditions and missions that a particular radar produces performance for the network greater than a notional equal benefit case. This allows the ordering of priority of radar tasking when tracking each flight. New Caledonia performs well for most flights; however, New Zealand is superior for ADL to SYD in winter as expected, being physically closer.

Informed by this, one may then adjust the mission planning of each radar. We may task the Norfolk Island radar to cover westward flights, the New Zealand radar to include the northern flights, and the New Caledonia radar to involve the southern-directed flights.

Alternatively, a radar may be removed with a reduced network mission scope, or radar systems may be added to increase the di-

versity of the geometry of propagation and flights. We may use the radar utility to prioritise the overall importance of a particular radar in the network. This could allow the removal of the Norfolk radar, as it performs particularly poorly in the worst environmental conditions of winter. We may then add another radar in a configuration to fill the BNE to SYD performance gap, such as Tasmania. This would provide a significant boost to the network performance due to the complementary radar geometry to the target area.

The radar utility may also guide maintenance schedules or the delivery order of building new radars. New Caledonia should be prioritised as the first radar built, as it provides the largest benefit with MEL to SYD and HBA to SYD superiority, where the majority of flights in Australia take place. We predict that significant maintenance of the New Zealand radar should be performed in summer, as it provides the most benefit in the difficult winter environmental conditions.

## CONCLUSION

We have considered the problem of designing a network of OTHR. We have assumed that the radars within this network have overlapping coverage and aspect and range diversity for the region of network coverage and a defined operational mission. The approach uses models for the individual radar design and the detection and tracking performance of each radar. The propagation and the noise environment are represented by using climatological models, and detailed propagation data are generated by using ray-tracing methods applied to the ionospheric climatological model. The radar network design methodology generates estimates for the median number of hours per day of effective radar performance and extends these for the total network performance. An estimate of the performance as a function of time of day can also be determined. Finally, a radar marginal utility metric is computed, and this is useful for understanding the rela-

tive contribution of each radar within the network. We have applied the approach to a hypothetical three-radar network and examined network performance for various radar sensitivity levels. In our example, the base-system design is shown to be poor, while higher sensitivity designs demonstrate improved network performance in mission-focused quantified metrics. ♦

### ACKNOWLEDGMENTS

The authors acknowledge earlier work in the area conducted by staff of the Defence Science and Technology Group, Australia, and the Relocatable Over-the-Horizon Radar system Program Office, Philadelphia, PA.

### REFERENCES

- [1] Skolnik, M. I. *Radar Handbook* (3rd ed.). New York: McGraw-Hill, 2008.
- [2] Davies, K. *Ionospheric Radio*. London, United Kingdom: Peregrinus, 1990.
- [3] Cameron, A. The Jindalee Operational Radar Network: Its architecture and surveillance capability. In *Proceedings of the IEEE International Radar Conference*, Alexandria, VA, 1995, 692–697.
- [4] Lomasney, J. M., and Sweeney, L. E., Jr. The twin-whip endfire receiving pair TWERP. Stanford Research Institute, Menlo Park, CA, Tech. Rep. IDL-TN-3, Oct. 1973.
- [5] Burke, G., Poggio, A., Logan, J., and Rockway, J. NEC—Numerical Electromagnetics Code for antennas and scattering. In *Proceedings of the Antennas and Propagation Society International Symposium*, Seattle, WA, June 1979, 147–150.
- [6] Bilitza, D., Altadill, D., Zhang, Y., Mertens, C., Truhlik, V., Richards, P., et al. The International Reference Ionosphere 2012—a model of international collaboration. *Journal of Space Weather and Space Climate*, Vol. 4 (2014), 1–12.
- [7] Cervera, M. A., and Harris, T. J. Modeling ionospheric disturbance features in quasi-vertically incident ionograms using 3-D magneto-ionic ray tracing and atmospheric gravity waves. *Journal Geophysical Research: Space Physics*, Vol. 119 (2014), 431–440.
- [8] George, P. L., and Bradley, P. A. A new method of predicting the ionospheric absorption of high frequency waves at oblique incidence. *Telecommunication Journal*, Vol. 41 (1974), 307–311.
- [9] Knott, E. F., Shaeffer, J. F., and Tuley, M. T. *Radar Cross Section* (2nd ed.). Boston: Artech House, 1993.
- [10] Union, I. T. Recommendation ITU-R P.372-11. Radio noise. International Telecommunication Union, Geneva, Switzerland, Tech. Rep., 2013.
- [11] Pederick, L. H., and Cervera, M. A. A directional HF noise model: calibration and validation in the Australian region. *Radio Science*, Vol. 51 (2016), 25–39.
- [12] Earl, G., and Ward, B. The frequency management system of the Jindalee over-the-horizon backscatter HF radar. *Radio Science*, Vol. 22, 2 (1987), 275–291.
- [13] Pederick, L. H., and Cervera, M. A. Modeling the interference environment in the HF band. *Radio Science*, Vol. 51 (2016), 82–90.
- [14] Swerling, P. Probability of detection for fluctuating targets. *IRE Transactions on Information Theory*, Vol. 6, 2 (1960), 269–308.
- [15] Davey, S. SNR limits on Kalman filter detect-then-track. *IEEE Signal Processing Letters*, Vol. 20, 8 (2013), 767–770.
- [16] Limentani, G., Ringo, M., Ye, F., Bergquist, M., and MCSorley, E. Beyond the t-test: statistical equivalence testing. *Analytical Chemistry*, Vol. 77, 11 (2005), 221A–226A.